

NEW RESULTS ON THE SUBMILLIMETER POLARIZATION SPECTRUM OF THE ORION MOLECULAR CLOUD

JOHN E. VAILLANCOURT,¹ C. DARREN DOWELL,^{1,2} ROGER H. HILDEBRAND,^{3,4} LARRY KIRBY,³ MEGAN M. KREJNY,⁵
HUA-BAI LI,⁶ GILES NOVAK,⁵ MARTIN HOUDE,⁷ HIROKO SHINNAGA,⁸ AND MICHAEL ATTARD⁷

submitted to ApJ Letters

ABSTRACT

We have used the SHARP polarimeter at the Caltech Submillimeter Observatory to map the polarization at wavelengths of 350 and 450 μm in a $\sim 2' \times 3'$ region of the Orion Molecular Cloud. The map covers the brightest region of the OMC-1 ridge including the Kleinmann-Low (KL) nebula and the submillimeter source Orion-south. The ratio of 450-to-350 μm polarization is $\sim 1.3 \pm 0.3$ in the outer parts of the cloud and drops by a factor of 2 towards KL. The outer cloud ratio is consistent with measurements in other clouds at similar wavelengths and confirms previous measurements placing the minimum of the polarization ratio in dusty molecular clouds at $\lambda \sim 350 \mu\text{m}$.

Subject headings: dust, extinction — ISM: clouds — ISM: individual (OMC-1) — polarization — submillimeter

1. INTRODUCTION

Studies of the wavelength dependence of interstellar polarization are common place in the near-visible region of the spectrum (e.g., Serkowski 1958; Martin & Whittet 1990; Martin, Clayton, & Wolff 1999; Whittet 2004). Such studies have put constraints on the mechanisms of magnetic grain alignment (Roberge 2004; Lazarian 2003, 2007) as well as the properties of dust grains responsible for interstellar extinction (e.g., Hildebrand & Dragovan 1995; Andersson & Potter 2007; Whittet et al. 2008; and references therein). There are fewer studies of the wavelength dependence at far-infrared and submillimeter wavelengths ($\sim 0.1 - 1 \text{ mm}$) where dust grains are responsible for most of the observed emission in Galactic clouds.

The first studies of multi-wavelength far-infrared/submillimeter polarimetry found unexpected results. Rather than a featureless spectrum due to a single population of dust grains, the polarization spectrum is observed to fall from 60 to 100 to 350 μm before rising again to 850 and 1300 μm (Hildebrand et al. 1999; Vaillancourt 2002, 2007). This spectral structure is attributed to the existence of multiple dust grain populations whose polarizability or alignment efficiency is correlated with either the grain temperature, the spectral dependence of the emissivity (the “spectral index”), or a combination of both. However, the existing data are quite sparse in terms of both wavelength coverage and the types of ob-

jects observed (bright Galactic clouds). Therefore, rather than pursue observations with the ability to test specific physical models, our immediate goal is to improve the empirical description of the spectrum by measuring the polarization at additional wavelengths between 100 and 850 μm which bracket the observed minimum at 350 μm .

To further this goal we have begun a campaign to measure the polarization of Galactic clouds at both 350 and 450 μm using SHARP, the SHARC-II polarimeter at the Caltech Submillimeter Observatory on the summit of Mauna Kea. While this is a fairly short wavelength baseline, such measurements will further constrain the location of the polarization minimum. For example, one can simply ask whether the minimum is less than, greater than, or approximately equal to 350 μm . This will place additional constraints on the possible range of polarizations, temperatures, and emissivities of the constituent grain populations (e.g., Hildebrand & Kirby 2004).

We have carried out the first set of observations for this project towards the Orion Molecular Cloud (OMC-1), a bright and well-studied region of massive star formation (e.g., Houde et al. 2004; Johnstone & Bally 1999; Lis et al. 1998). In §2 below we review the SHARP instrument and the polarimetric/photometric observations. Maps are presented in §3 followed by a discussion of the polarization spectrum in §4.

2. OBSERVATIONS AND DATA REDUCTION

SHARP (Li et al. 2006, 2008; Novak et al. 2004) is a fore-optics module that installs onto the SHARC-II camera. Incident radiation is split into two orthogonally polarized beams which are then imaged onto opposite ends of the 12×32 pixel SHARC-II bolometer array. The result is a dual-polarization 12×12 pixel polarimeter with a $55'' \times 55''$ field of view (FOV). The polarization is modulated by stepping a half-wave plate (HWP) at the relative angles 0, 22.5, 45, and 67.5 degrees.

Within each FOV and HWP position, standard photometric beam-switching was performed with a chop throw of $5'$ and a chop position angle in the range $80^\circ - 150^\circ$ east of north. This is repeated at positions separated by $50''$ in right ascension and declination to

¹ Division of Physics, Mathematics, & Astronomy, California Institute of Technology, MS 320-47, 1200 E. California Blvd., Pasadena, CA 91125

² also Jet Propulsion Laboratory

³ Enrico Fermi Institute and Department of Astronomy & Astrophysics, University of Chicago, 5640 S. Ellis Ave., Chicago, IL 60637

⁴ also Department of Physics

⁵ Department of Physics and Astronomy, Northwestern University, 2145 Sheridan Rd., Evanston, IL 60208

⁶ Harvard-Smithsonian Center for Astrophysics, 60 Garden St., MS-78, Cambridge, MA 02138

⁷ Department of Physics and Astronomy, University of Western Ontario, London, ON, Canada N6A 3K7

⁸ Caltech Submillimeter Observatory, 111 Nowelo St., Hilo, HI 96720

build maps larger than the FOV. For this work we have generated maps of size $2' \times 3'$ encompassing the 2 brightest submillimeter cores in OMC-1 (the Kleinmann-Low nebula, hereafter KL; and the submillimeter source of Keene, Hildebrand, & Whitcomb (1982) sometimes called Orion-south, hereafter KHW). Observations at 350 and 450 μm were carried out on 2007 February 16 and 2006 December 5, respectively.

The generation of Stokes parameters, polarization amplitudes, and position angles within each single set of 4 HWP angles follows the same general procedures outlined by Platt et al. (1991) and Hildebrand et al. (2000). Maps of the linear Stokes parameters I, Q, and U are generated from the dithered and stepped array positions by interpolating the data onto a finer grid and coadding (e.g., Houde & Vaillancourt 2007).

The polarization data presented in §3 have been corrected for positive bias (Simmons & Stewart 1985; Vaillancourt 2006) and for measured polarization efficiencies of 93% and 98% at 350 and 450 μm , respectively. The data have also been corrected for instrument polarizations of $\approx 0.3\text{--}0.5\%$ at 350 μm and $\lesssim 0.2\%$ at 450 μm (Li et al. 2008; Vaillancourt et al., in preparation). The polarization position angle calibration, measured by illuminating SHARP with an unpolarized source through a calibration grid, is accurate to within 2° .

We obtained photometric data at 350 μm using SHARC-II in camera mode on 2007 August 11–12. Four raster scans (without chopping) centered on Ori IRC2 were performed to cover a $\sim 10' \times 10'$ field. Flux maps were produced using the `sharc_solve`⁹ utility, which models the source flux, sky background fluctuations, instrument gains, and drifts in the instrument electronics. Absolute fluxes are calibrated with respect to the standard sources L 1551 and Mars (using peak flux estimates of 45.2 and 3.80×10^3 Jy per $9''$ FWHM beam, respectively)¹⁰ and have an uncertainty of $\sim 20\%$.

3. RESULTS

Figure 1 shows the polarimetric and photometric maps in the $\sim 2' \times 3'$ region covered by the polarization observations. The size of the gaussian smoothing kernel used to interpolate the 350 μm polarization data has been chosen so that the resulting resolution matches that of the 450 μm polarization data ($13''$ FWHM). Figures 1a–c plot the 350 and 450 μm polarization results over a contour map of total flux measured at 350 μm . At each wavelength we plot vectors at an interval of $9/5$ (Figs. 1a–b).

Figure 1a shows the polarization results with the length of the vector proportional to the measured polarization amplitude and the position angle parallel to the polarization vector. The most obvious feature of this map is the decrease in the polarization amplitude (at both wavelengths) towards the KL intensity peak, and to a lesser extent towards KHW. This so-called “polarization hole” effect in which the polarization drops towards intensity peaks has been observed in these and other sources by experiments at a range of far-infrared

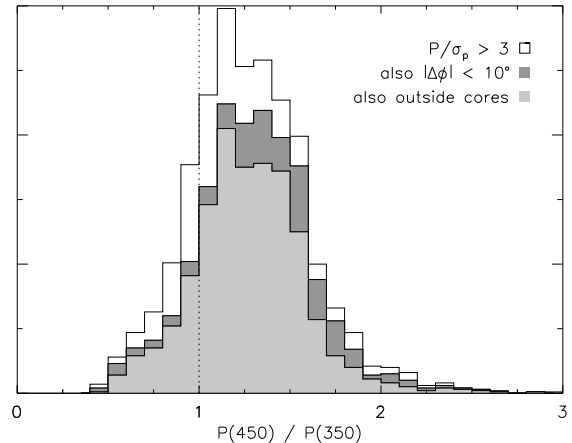


Fig. 2.— Histogram of the 450/350 μm polarization ratio. All data shown here have been limited to only those points where $P \geq 3\sigma_p$ at both wavelengths. Also shown are histograms where data points satisfy the additional criteria that the position angle rotates by less than 10° between the two wavelengths ($|\Delta\phi| < 10^\circ$) and that the points are at least $20''$ away from the two submillimeter flux peaks KL and KHW.

and submillimeter wavelengths (e.g., Schleuning 1998; Coppin et al. 2000; Matthews et al. 2001; Dotson et al. 2000, 2008).

In Figure 1b we have rotated the polarization vectors by 90° to show the inferred magnetic field direction. The plotted \mathbf{B} -vectors are drawn with a constant length (not proportional to polarization amplitude) in order to more clearly observe the position angle differences across the map and between the two wavelengths. The position angles exhibit a clockwise rotation with increasing wavelength, differing by more than 25° around KL and the region immediately east (less than 1% of the data exhibit larger changes). This angular rotation is much smaller to the west and south of KL. The larger variation of the position angle with wavelength towards KL than along the ridge between KL and KHW is also clearly seen when the data are compared with observations at 850 μm (not shown, but see e.g., Matthews et al. 2003).

The color scale of Figure 1c shows the ratio of the polarization amplitude at the two wavelengths, $P(450)/P(350)$. Most points in the map exhibit a two-point polarization spectrum which increases with wavelength, $P(450)/P(350) > 1$ (Fig. 2). The most obvious exceptions are towards KL and the region to its northwest. KHW does not exhibit a similar drop in the polarization ratio.

4. DISCUSSION

4.1. Minimum in the Polarization Spectrum

Examining SHARP data at only points outside the KL and KHW intensity peaks (beyond a $20''$ radius) we find a median in the distribution of $P(450)/P(350) = 1.3 \pm 0.3$, where the uncertainty represents the standard deviation of those points (Fig. 2). This data point is consistent with a simple interpolation of data from other Galactic clouds at wavelengths of 350 and 850 μm (Fig. 3). (Note that Fig. 3 also includes data at 850 μm from the Galactic cloud W51 (Chrysostomou et al. 2002), not available at the time of the Vaillancourt (2002) compilation; the comparison between the 850 μm SCUBA data and the 350 μm Hertz data (Dotson et al. 2008) is performed as

⁹ [http://www.submm.caltech.edu/~sim\\$sharc/analysis/overview.htm](http://www.submm.caltech.edu/~sim$sharc/analysis/overview.htm)

No significant differences were seen between maps reduced using `sharc_solve` and those reduced using `CRUSH` ([http://www.submm.caltech.edu/~sim\\$sharc/crush/](http://www.submm.caltech.edu/~sim$sharc/crush/)).

¹⁰ [http://www.submm.caltech.edu/~sim\\$sharc/analysis/calibration.htm](http://www.submm.caltech.edu/~sim$sharc/analysis/calibration.htm)

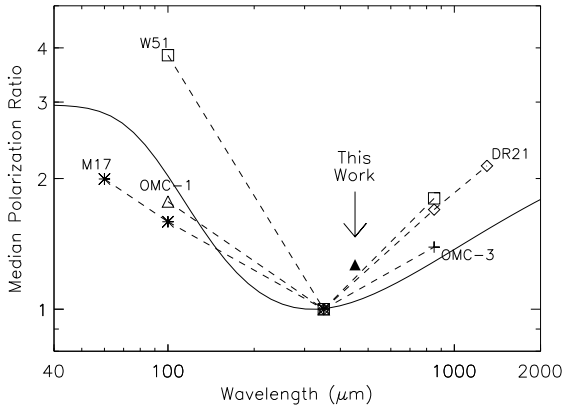


FIG. 3.— Far-infrared and submillimeter polarization spectrum, normalized at $350 \mu\text{m}$. The $450/350 \mu\text{m}$ OMC-1 comparison from this work is shown as a solid triangle. The $850/350 \mu\text{m}$ comparison in W51 (open squares) is calculated from $850 \mu\text{m}$ data in Chrysostomou et al. (2002) and $350 \mu\text{m}$ data in Dotson et al. (2008). All other data are from Vaillancourt (2002). The solid curve is a 2-component dust model (see text).

outlined in Vaillancourt (2002).) From the results of Figure 3, and assuming that the polarization spectrum in OMC-1 is similar to that of other clouds (i.e., it continues to rise at wavelengths greater than $450 \mu\text{m}$), we estimate that the minimum in the spectrum cannot occur at wavelengths much less than $350 \mu\text{m}$.

4.2. Polarization Ratio in Different Environments

Given the low polarization ratio towards KL compared with the rest of the cloud, it is natural to ask if this may be due to some unique physical condition as compared with the remainder of the cloud. At the very least, it is obvious that KL is the region with the highest flux density in the cloud. To examine this trend, we plot the $450/350$ polarization ratio as a function of $350 \mu\text{m}$ flux F_{350} . Figure 4 plots the polarization data as individual points (dots) and combined into equal-sized logarithmic flux bins (diamonds). At low fluxes ($F_{350} \lesssim 50\%$ of the peak flux) the polarization ratio clusters about $P(450)/P(350) \approx 1.2 - 1.5$ with a large scatter (this distribution is best shown in the histogram of Figure 2). At larger fluxes the binned data show a sharp drop in the polarization ratio. The flux level at which this drop occurs is indicated by the thick contours in Figure 1c. With few exceptions all data above this flux level lie in KL. The binned data in Figure 4 drop below $P(450)/P(350) = 1$ for $F(350) \gtrsim 60\%$. At this flux level all points are within $\sim 20''$ of KL.

Polarized emission from dust grains all with the same temperature results in a nearly constant polarization spectrum in the wavelength range $50 - 2000 \mu\text{m}$ (Hildebrand et al. 1999). A spectrum such as that in Figure 3, or points in Figure 4 with $P(450)/P(350) \neq 1$, requires the existence of at least two dust-emission components (Hildebrand et al. 1999; Vaillancourt 2002). Such a polarization spectrum is modeled in Figure 3. This model has a minimum at $330 \mu\text{m}$ and uses optically thin dust with temperatures $T = 20$ and 50 K, spectral indices $\beta = 2$ and 1 , respectively,¹¹ and peak fluxes in the ratio $F_{\text{cold}}/F_{\text{hot}} = 0.5$. The cold component is unpolar-

¹¹ An inverse T - β relation is observed to be typical for dust in molecular clouds (e.g., Dupac et al. 2001, 2003).

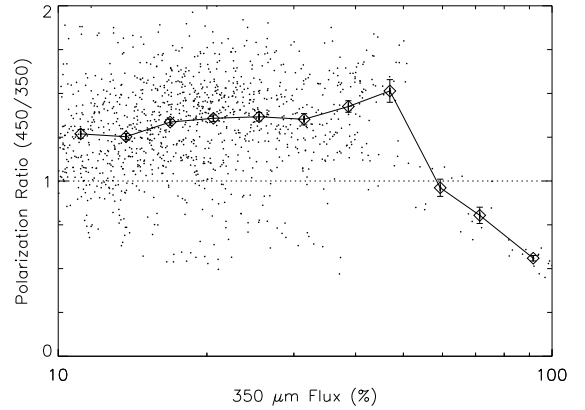


FIG. 4.— Polarization ratio ($450 / 350 \mu\text{m}$) vs. the total $350 \mu\text{m}$ flux (percentage of peak flux). Dots indicate individual measurements within the maps of Figure 1c while diamonds represent an average of the plotted quantity over logarithmic bins of $350 \mu\text{m}$ flux. Error bars on the polarization ratio represent the standard deviation of the mean within each bin.

ized while the warm component is polarized. While a two-component dust model for molecular clouds is physically unrealistic, it is sufficient to illustrate how a multi-component model can explain the empirical results.

Even with only 2 components, small adjustments to the parameters allow for better agreement between the model and the specific data points of Figure 3. A spectral energy distribution (SED) dominated by cold unpolarized dust ($F_{\text{cold}}/F_{\text{hot}} \gg 1$) can reproduce the ratio observed in the OMC-1 cloud envelope, $P(450)/P(350) \approx 1.3$. Such an SED will appear nearly-isothermal if the measurement uncertainties are large and/or it is not sufficiently sampled in wavelength space. This is consistent with the analysis of Vaillancourt (2002) where no significant evidence is seen for multiple dust temperatures outside of KL or the M42 H II region, but where the polarization spectrum is still observed to change with wavelength.

The KL region is quite massive and contains high column densities of both warm ($T \gtrsim 40$ K) and cold ($T \lesssim 25$ K) dust. As a result, emission from cold and warm dust contribute nearly equally to the total flux observed at 350 and $450 \mu\text{m}$. The coldest ($T \approx 20$ K) and warmest ($T \approx 45$ K) regions of OMC-1 are regions towards KL and KHW (Vaillancourt 2002). As one moves towards KL from within $30''$ of the peak the temperature of the cold component decreases by ~ 2 K, and the warm component increases by ~ 3 K. These modest temperature changes are enough to shift the polarization minimum by as much as $70 - 130 \mu\text{m}$ (depending on the relative spectral indices of the components); moving to longer wavelengths towards the intensity peak.

Therefore, we expect the polarization minimum to shift to longer wavelengths at the larger flux values towards the KL peak. If the observed wavelengths are near the minimum then we expect the $450/350$ ratio to decrease from a value greater than unity when the minimum is below $400 \mu\text{m}$, to a value approximately equal to one when the minimum is bracketed by the two observed wavelengths, and to continue to decrease below one as the minimum moves to wavelengths greater than $400 \mu\text{m}$. This is the trend observed in Figure 4 for points with $F_{350} \gtrsim 50\%$.

4.3. Summary and Future Work

By comparing the 450/350 μm polarization ratio in OMC-1 with that in other bright Galactic clouds (Fig. 3) we estimate that the minimum in the polarization spectrum is not much less than 350 μm . However, given the variation in 60 – 1300 μm polarization spectrum from cloud-to-cloud, we do not draw strong conclusions about the polarization minimum in any cloud other than OMC-1. We are continuing our campaign to observe and analyze other bright clouds in a manner similar to that described here.

The existence of a minimum in the far-infrared/submillimeter polarization spectrum, as opposed to a simple rise or fall from one end of the spectrum to the other, implies either (a) the existence of more than 2 dust temperature components, and/or (b) a change in the dust emissivity index as well as its temperature. Multi-wavelength observations in the far-infrared (50 – 200 μm ; Dotson et al. 2000;

Dowell et al. 2003; Vaillancourt et al. 2007) or submillimeter ($> 450 \mu\text{m}$; Curran & Chrysostomou 2007; Bastien, Jenness, & Molnar 2005; Matthews et al., in preparation) at wavelengths on only one side of this minimum are insufficient for studying this behavior. SHARP (at 350 and 450 μm) therefore occupies a unique niche for studies of the polarization spectrum by providing a link between these two wavelength extremes.

We are grateful for the help of the Caltech Submillimeter Observatory (CSO) staff in installing and observing with SHARP and SHARC-II. Also thanks to Jackie Davidson, and Emeric LeFloc'h for observing assistance. SHARP has been supported by NSF grants AST 02-41356, AST 05-05230, and AST 05-05124. The CSO is supported by the NSF through grant AST 05-40882.

Facilities: CSO (SHARC2).

REFERENCES

- Andersson, B.-G. & Potter, S. B. 2007, *ApJ*, 665, 369
 Bastien, P., Jenness, T., & Molnar, J. 2005, in *ASP Conf. Ser.* 343, *Astronomical Polarimetry — Current Status and Future Directions*, ed. A. Adamson, 69
 Chrysostomou, A., Aitken, D. K., Jenness, T., Davis, C. J., Hough, J. H., Curran, R., & Tamura, M. 2002, *A&A*, 385, 1014
 Coppin, K. E. K., Greaves, J. S., Jenness, T., & Holland, W. S. 2000, *A&A*, 356, 1031
 Curran, R. L. & Chrysostomou, A. 2007, *MNRAS*, 382, 699
 Dotson, J. L., Davidson, J., Dowell, C. D., Schleuning, D. A., & Hildebrand, R. H. 2000, *ApJS*, 128, 335
 Dotson, J. L., Davidson, J. A., Dowell, C. D., Hildebrand, R. H., Kirby, L., & Vaillancourt, J. E. 2008, *ApJS*, submitted
 Dowell, C. D., Davidson, J. A., Dotson, J. L., Hildebrand, R. H., Novak, G., Rennick, T. S., & Vaillancourt, J. E. 2003, in *Proc. SPIE 4843, Polarimetry in Astronomy*, ed. S. Fineschi (SPIE), 250
 Dupac, X., et al. 2001, *ApJ*, 553, 604
 —. 2003, *A&A*, 404, L11
 Hildebrand, R. & Kirby, L. 2004, in *ASP Conf. Ser.* 309, *Astrophysics of Dust*, ed. A. N. Witt, G. C. Clayton, & B. T. Draine (San Francisco: ASP), 515
 Hildebrand, R. H., Davidson, J. A., Dotson, J. L., Dowell, C. D., Novak, G., & Vaillancourt, J. E. 2000, *PASP*, 112, 1215
 Hildebrand, R. H., Dotson, J. L., Dowell, C. D., Schleuning, D. A., & Vaillancourt, J. E. 1999, *ApJ*, 516, 834
 Hildebrand, R. H. & Dragovan, M. 1995, *ApJ*, 450, 663
 Houde, M., Dowell, C. D., Hildebrand, R. H., Dotson, J. L., Vaillancourt, J. E., Phillips, T. G., Peng, R., & Bastien, P. 2004, *ApJ*, 604, 717
 Houde, M. & Vaillancourt, J. E. 2007, *PASP*, 119, 871
 Johnstone, D. & Bally, J. 1999, *ApJ*, 510, L49
 Keene, J., Hildebrand, R. H., & Whitcomb, S. E. 1982, *ApJ*, 252, L11
 Lazarian, A. 2003, *J. Quant. Spectros. Radiat. Transfer*, 79, 881
 —. 2007, *J. Quant. Spectros. Radiat. Transfer*, 106, 225
 Li, H., Attard, M., Dowell, C. D., Hildebrand, R. H., Houde, M., Kirby, L., Novak, G., & Vaillancourt, J. E. 2006, in *Proc. SPIE 6275, Millimeter and Submillimeter Detectors and Instrumentation for Astronomy III*, ed. J. Zmuidzinas, W. S. Holland, S. Withington, & W. D. Duncan, 62751H
 Li, H., Dowell, C. D., Kirby, L., Novak, G., & Vaillancourt, J. E. 2008, *Appl. Opt.*, 47, 422
 Lis, D. C., Serabyn, E., Keene, J., Dowell, C. D., Benford, D. J., Phillips, T. G., Hunter, T. R., & Wang, N. 1998, *ApJ*, 509, 299
 Martin, P. G., Clayton, G. C., & Wolff, M. J. 1999, *ApJ*, 510, 905
 Martin, P. G. & Whittet, D. C. B. 1990, *ApJ*, 357, 113
 Matthews, B. C., Chuss, D., Dotson, J., Dowell, D., Hildebrand, R., Johnstone, D., & Vaillancourt, J. 2003, in *Chemistry as a Diagnostic of Star Formation*, ed. C. L. Curry & M. Fich, 145
 Matthews, B. C., Wilson, C. D., & Fiege, J. D. 2001, *ApJ*, 562, 400
 Novak, G., et al. 2004, in *Proc. SPIE 5498, Millimeter and Submillimeter Detectors for Astronomy II*, ed. J. Zmuidzinas, W. S. Holland, & S. Withington, 278
 Platt, S. R., Hildebrand, R. H., Pernic, R. J., Davidson, J. A., & Novak, G. 1991, *PASP*, 103, 1193
 Roberge, W. G. 2004, in *ASP Conf. Ser.* 309, *Astrophysics of Dust*, ed. A. N. Witt, G. C. Clayton, & B. T. Draine (San Francisco: ASP), 467
 Schleuning, D. A. 1998, *ApJ*, 493, 811
 Serkowski, K. 1958, *Acta Astron.*, 8, 135
 Simmons, J. F. L. & Stewart, B. G. 1985, *A&A*, 142, 100
 Vaillancourt, J. E. 2002, *ApJS*, 142, 53
 —. 2006, *PASP*, 118, 1340
 —. 2007, in *EAS Publ. Ser.* 23, *Sky Polarisation at far-infrared to radio wavelengths: The Galactic Screen before the Cosmic Microwave Background*, ed. F. Boulanger & M.-A. Miville-Deschênes (EDP Sciences), 147
 Vaillancourt, J. E., et al. 2007, in *Proc. SPIE 6678, Infrared Spaceborne Remote Sensing and Instrumentation XV*, ed. M. Strojnik, 6678-0D
 Whittet, D. C. B. 2004, in *ASP Conf. Ser.* 309, *Astrophysics of Dust*, ed. A. N. Witt, G. C. Clayton, & B. T. Draine (San Francisco: ASP), 65
 Whittet, D. C. B., Hough, J. H., Lazarian, A., & Hoang, T. 2008, *ApJ*, 674, 304

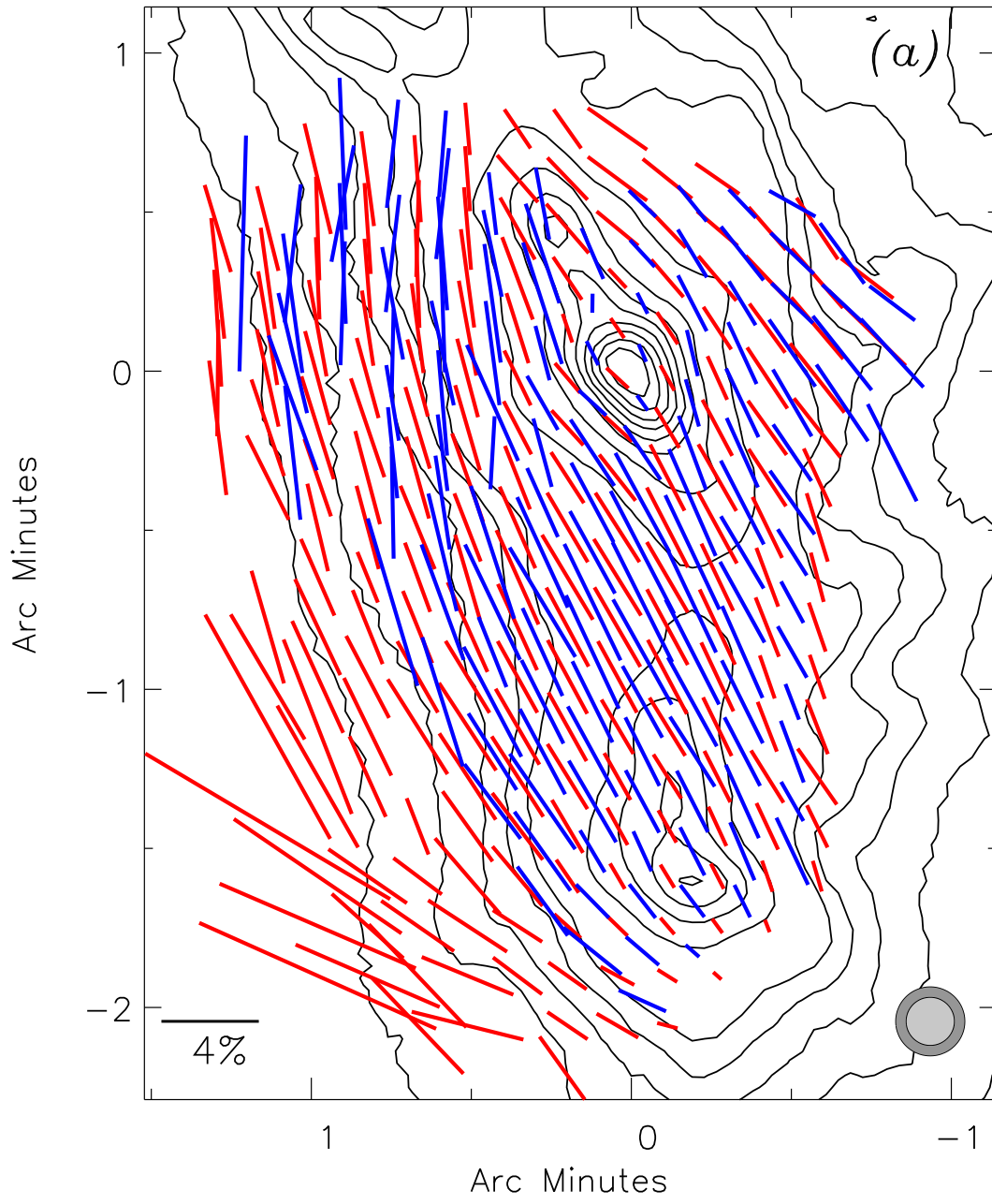


Figure 1a

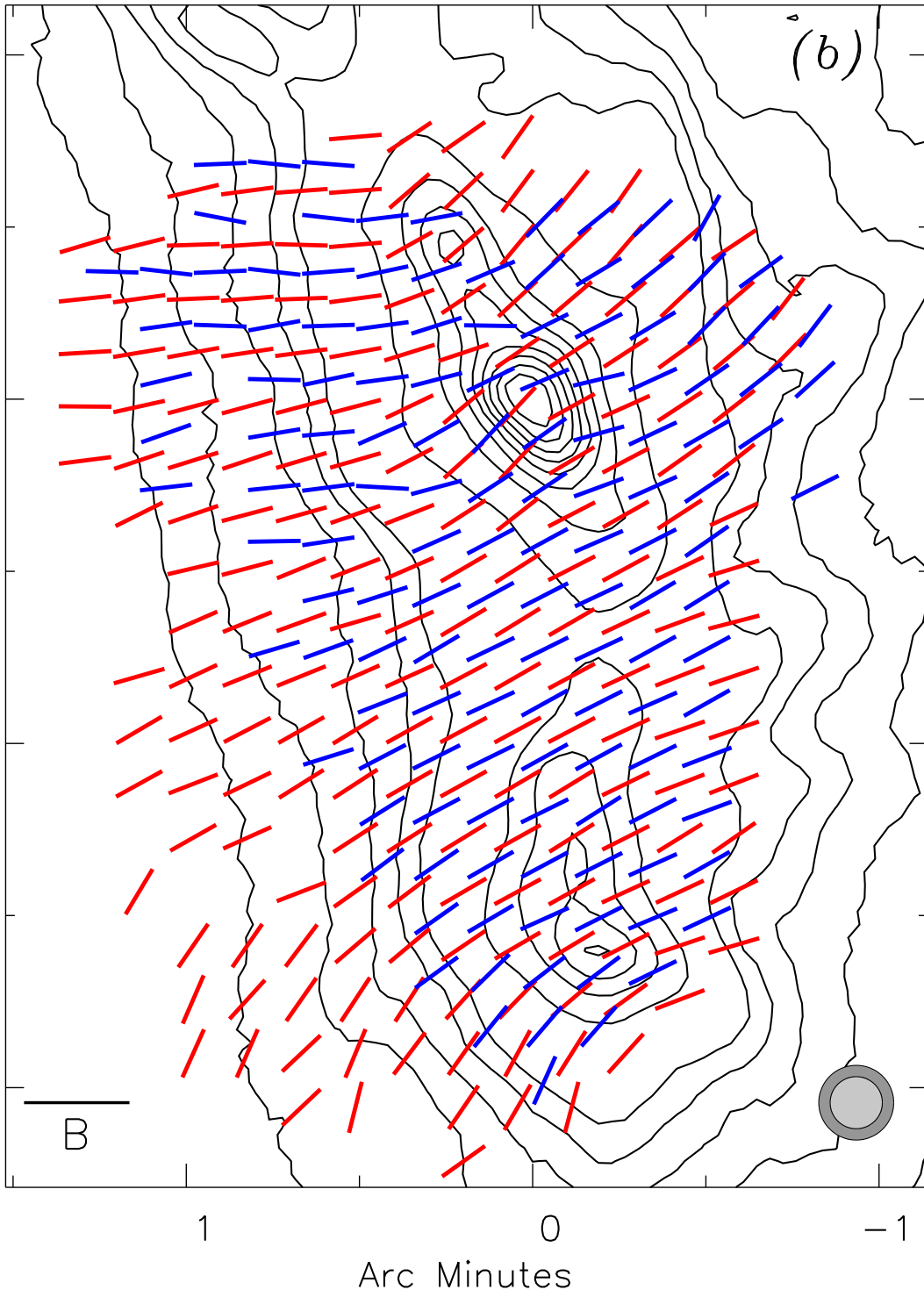


Figure 1b

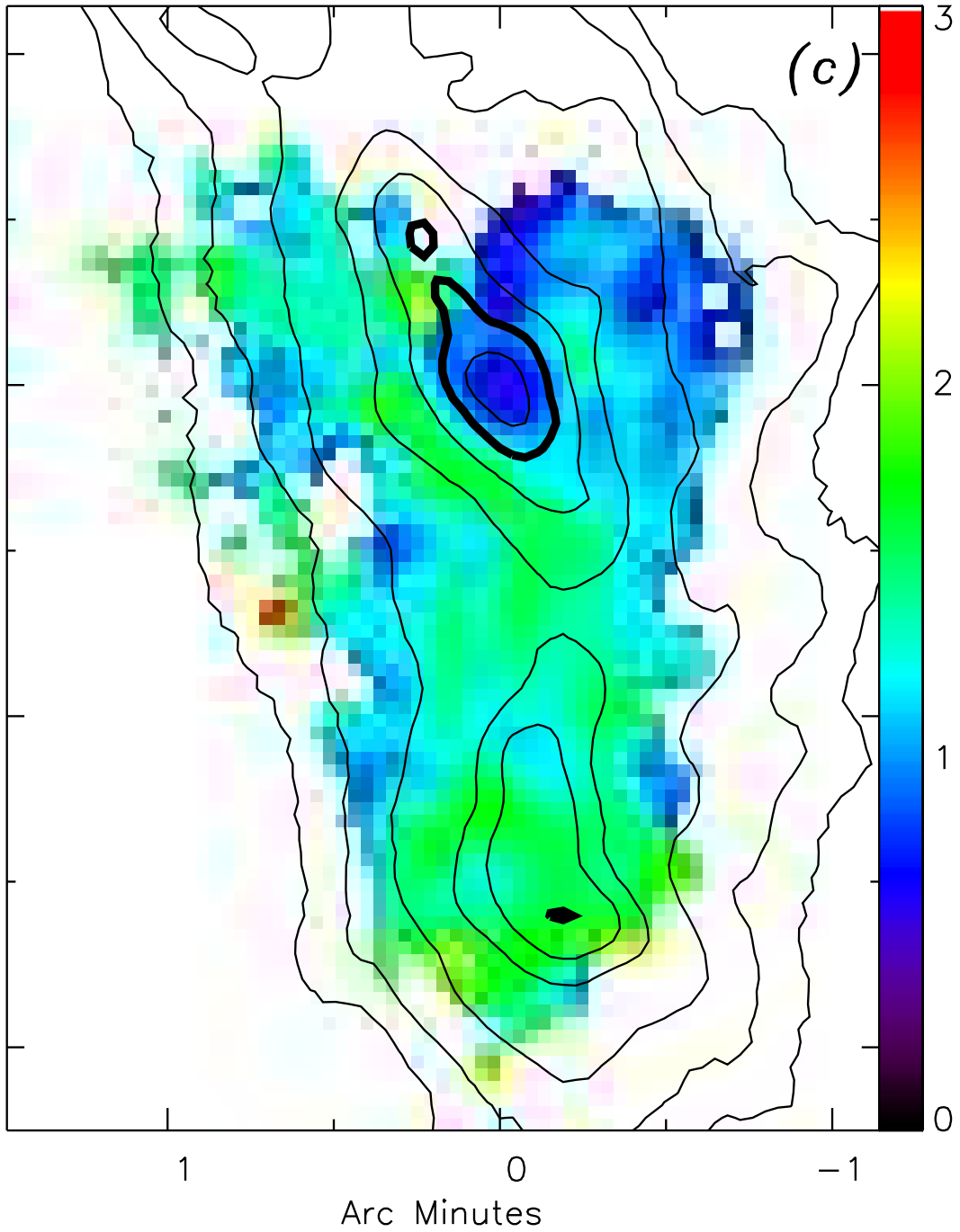


Figure 1c

FIG. 1.— Polarimetric and photometric maps of OMC-1. Effective beamsizes (FWHM) for the photometric ($9''$) and polarimetric ($13''$) observations are shown as gray circles in (a) and (b). Coordinate offsets are measured with respect to Ori IRC2 at $5^{\text{h}}35^{\text{m}}14.5^{\text{s}}$, $-5^{\circ}22'31''$ (J2000). KL is the northernmost flux peak coincident with the coordinate origin and KHW/Orion-south is the peak $\sim 1'.5$ to the south. Only polarization data satisfying $P > 3\sigma_p$ are included. a) 350 (red) and 450 (blue) μm polarization vectors superposed on 350 μm flux contours. Contours are drawn at 2, 4, 6, 8, 10, 20, ..., and 90% of the peak (≈ 780 Jy per $9''$ beam). b) Inferred magnetic field vectors at 350 and 450 μm drawn with a constant length (i.e., not proportional to the polarization amplitude); contours as in (a). c) The color scale shows the polarization ratio between the two wavelengths, $P(450)/P(350)$. Contours at 350 μm are drawn at 4, 6, 10, 20, 30, 50, and 80% of the peak flux; the 50% contour is drawn thicker (see Fig. 4).